Journal of Power Sources 195 (2010) 7332–7337

Contents lists available at ScienceDirect

Journal of Power Sources

journal homepage: www.elsevier.com/locate/jpowsour

Design, fabrication and performance evaluation of a miniature air breathing direct formic acid fuel cell based on printed circuit board technology

Ping Hong, Shijun Liao, Jianhuang Zeng*, Xinjian Huang

School of Chemistry and Chemical Engineering, South China University of Technology, Guangzhou 510641, China

ARTICLE INFO

Article history:
Received 13 April 2010
Received in revised form 12 May 2010
Accepted 12 May 2010
Available online 19 May 2010

Keywords:
Direct formic acid fuel cell (DFAFC)
Air breathing
Printed circuit board (PCB)

ABSTRACT

A miniature air breathing compact direct formic acid fuel cell (DFAFC), with gold covered printed circuit board (PCB) as current collectors and back boards, is designed, fabricated and evaluated. Effects of formic acid concentration and catalyst loading (anodic palladium loading and cathodic platinum loading) on the cell performance are investigated and optimized fuel concentration and catalyst loading are obtained based on experimental results. A maximum power density of 19.6 mW cm^{-2} is achieved at room temperature with passive operational mode when 5.0 M formic acid is fed and 1 mg cm^{-2} catalyst at both electrodes is used. The home-made DFAFC also displays good long-term stability at constant current density.

1. Introduction

Recently, increased interests have been paid to the use of miniature fuel cells as power sources for portable devices, such as personal digital assistants (PDAs), laptop computers and 3G phones et al. Amongst, miniature polymer electrolyte membrane fuel cells (PEMFCs) [1] and direct methanol fuel cells (DMFCs) [2–4] in particular, are regarded as the potential candidates for this purpose. In fact, the *FuelCellToday* market survey showed that 94% of the portable fuel cell market was attributed to DMFCs and PEMFCs [5]. However, methanol crossover is still a big problem for the application of DMFCs unless better methanol resistant membrane (relative to Nafion) is found [6,7]. Furthermore, the poisoning of anode catalysts caused by CO intermediates remains a big challenge. For H_2–O_2 PEMFCs, two obstacles that hampered their application are the high cost of hydrogen mini-storage and the potential safety concerns for the use and transportation of hydrogen [8,9]. Therefore, researchers begin to look for fuel cells operated on other fuels and these include formic acid, ethanol, dimethyl ether and so on [10].

Compared with other liquid fuel cells and H_2–O_2 PEMFCs, direct formic acid fuel cells (DFAFCs) have many advantages for micro power generation. Formic acid is a non-flammable and non-toxic liquid at room temperature; dilute formic acid is on the US Food and Drug Administration list of food additives as a preservative and antibacterial agent that is generally recognized as safe [11–13]. Formic acid is an easily available industry product that is produced as a by-product in the manufacture of acetic acid. The theoretical open-circuit potential (OCP) for DFAFCs is 1.45 V, higher than that of DMFC (1.18 V) and H_2–O_2 PEMFC (1.23 V) [14]. Formic acid also exhibits low crossover rate through Nafion membranes because of the repulsion between $HCOO^-$ in formic acid and sulfuric groups in the surface of Nafion membrane [7,13,15]. This allows for high level concentration tolerance, making up for its low theoretical power density (1700 Wh kg^{-1}). Recently research interests for DFAFCs are mainly focused on catalysts [16–18] and active cells [11,14,19–21]. A few studies have been reported on passive DFAFCs [22,23]. To the best of our knowledge, printed circuit board (PCB) has rarely been used as current collector for passive DFAFCs. There are many advantages of using PCB in the design. One advantage is to simply cell configuration. PCB used in this work consisted of an electroplated Au layer on Cu as current collector whereas the epoxy layer was used as end plate. The current collector and end plate were integrated in one PCB plate. In comparison, tradition passive fuel cells include separate end plate or holder, insulator and current collector [3,24,25]. Secondly, PCB board can be easily machined [26]. Conventionally used stainless steel or Ti board must incise (which is sophisticated and costly) as shown in the reference [25]. Thirdly, the thermal conductivity of PCB is lower than stainless steel or Ti and this merit is favorable for heat preservation leading to higher cell operating temperature. Lastly, using of PCB can reduce cell weight. The density of PCB is the smallest compared with stainless steel and Ti (Ti board: 4.5 g cm^{-3}, 316L stainless steel: 8.03 g cm^{-3}, fiberglass epoxy PCB: 2 g cm^{-3}), therefore the use of PCB can reduce cell weight significantly.

In this study, we developed a miniature air breathing DFAFC based on PCB technology. PCB with a thickness of 2.5 μm Au elec-

* Corresponding author. Tel.: +86 20 87113586/805; fax: +86 20 87112977.
E-mail address: cejhzeng@scut.edu.cn (J. Zeng).

0378-7753/$ – see front matter © 2010 Elsevier B.V. All rights reserved.
doi:10.1016/j.jpowsour.2010.05.024

troplated layer was used as current collector. Detailed design and fabrication of the cell with an active area of 4 cm^2 was described. The effects of formic acid concentration and catalyst loading on the cell performance were also discussed.

2. The cell configuration

2.1. Middle plate

The function of the middle plate was to store fuel and provide support to the cell. A polymethyl methacrylate (PMMA) board with a thickness of 8 mm, which was strong enough to support the cell and was also acid-resistant to prevent the cell eroding by formic acid, was used to fabricate the plate. Moreover, the thermal conductivity of PMMA is low (0.19 $W\,m^{-1}\,K^{-1}$), which favors heat preservation in the cell leading to higher cell operating temperature [25,27]. The square (2.1 mm × 2.1 mm) in the center served as the fuel reservoir with a total volume of about 3.5 ml. The surrounding area of the plate was evenly carved with 8 small circular holes (Ø 3 mm), so the stainless steel bolts can travel through them and hold the cell parts together. In the top of the plate, two circular holes (Ø 2 mm) were used as fuel entrance and gas exit. Formic acid as reactant was injected using a syringe through the hole to the fuel reservoir whereas CO_2 created during the reaction released to the environment via the hole.

2.2. Current collector

The current collector is an important part of the cell [28,29], which serves for conducting current and delivering fuel and oxygen. Conventional current collectors include titanium foil coated with gold [23,24], stainless steel plate [30] and graphite plates [31]. Coated titanium foil and stainless steel are corrosion resistant and stiff enough to endure large pressure applied between collector and electrode. However they are not lightweight at all. Light-weighted graphite plates, nevertheless, have very poor machinability especially for small-sized plates. In our work a PCB coated with gold was used as current collector both in anode and cathode, as is shown in Fig. 1. Gold coated PCB has sufficient stiffness and can be easily machined thus reducing the cell internal resistance and cell volume. One hundred and fourty-four circular holes (Ø 1 mm) were distributed evenly in the 2 cm × 2 cm board by digitally controlled drill. The open ratio is about 28%. The holes are for the passage of reactants and products. Reactants, formic acid and oxygen (air), can travel through them to the catalyst layers whereas products including CO_2 and water exit from the catalyst layers. Traditional PCB is coated as copper, which is not corrosion resistant to formic acid. To prevent corrosion, an Au layer with a thickness of 2.5 μm (detected by CMI560) was electroplated on the copper after the holes are drilled. The rest of the copper layer was etched away using etchant.

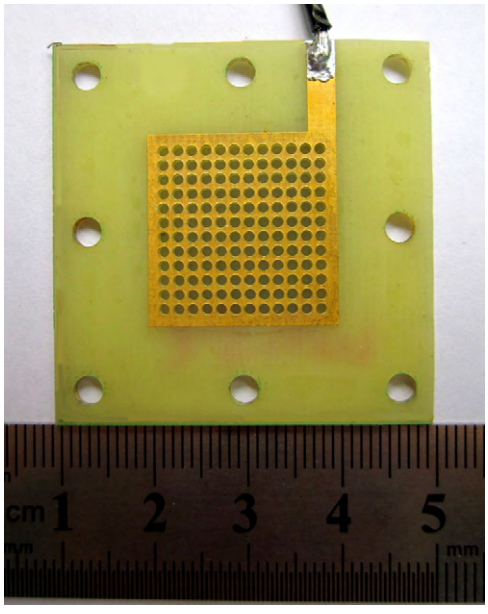

Fig. 1. Current collector based on PCB technology with a 2.5 μm thickness of Au-coated layer.

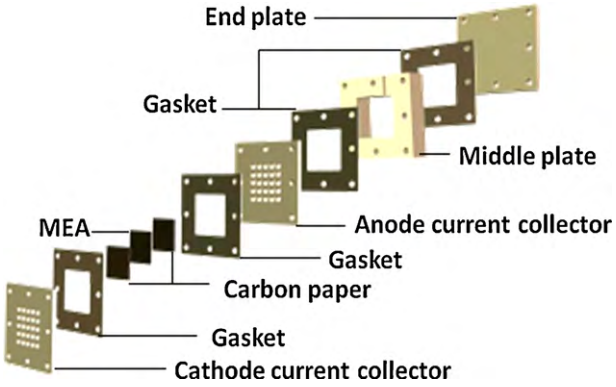

Fig. 2. Schematic of the cell.

2.3. Gasket

The gasket with appropriate thickness and material is crucial for insuring the cell sealing and reducing the contact resistance [25]. In this work we select silicon membrane with a thickness of 0.17 mm as the gasket. By the compression from the surrounding eight bolts, sufficient sealing and good contact between the current collector and catalyst layers can be achieved.

2.4. Integrated mini-cell

The middle plate, current collector, gasket discussed above and membrane electrode assembly (MEA), carbon papers (mentioned in the following experimental part) were assembled, as was shown in Fig. 2. Eight stainless steel bolts (Ø 3 mm × 20 mm) were used to secure adequate compression between the components. The purpose of the two thin copper wires (the red one was anode and the black one was cathode) which were connected to current collectors, was to export current for testing. The final assembled cell is showed in Fig. 3. The dimension of the cell was 4 cm by length, 3 cm by width and 4 cm by height.

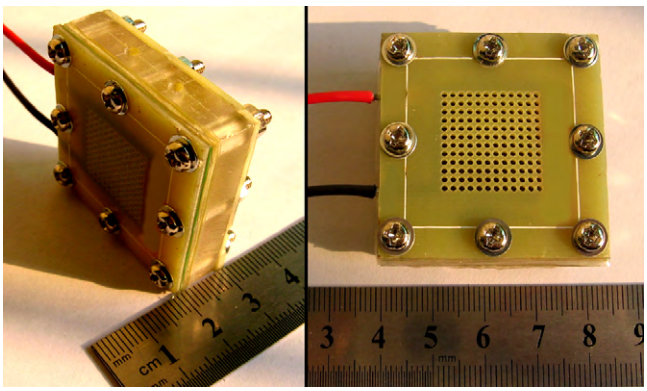

Fig. 3. Miniature air breathing DFAFC developed in this study.

3. Experimental

MEA, each with an active area of 4 cm^2, were fabricated using a 'direct catalyst spraying' technique. A certain amount of catalyst powders was dispersed into appropriate amounts of isopropyl alcohol (Sinopharm Chemical Reagent Co.,) and 5% Nafion solution (Dupont, 5 wt.% in alcohol). The 'inks', then, were sprayed onto each side of Nafion® 212 membrane (Dupont) using an air brush. The MEA was dried in vacuum oven at 70 °C overnight before usage. More detailed process can be found elsewhere [32]. Pt/C (Johnson Matthey, 40 wt.%) and Pd/C (home-made, 20 wt.%) [33] were used as cathode and anode catalysts respectively with a variant loading of 0.5–2 mg cm^{-2}. Carbon papers (E-TEK) used as diffusion layers without any pretreatment were sandwiched between the catalyst layers and current collectors.

The cell *I–V* curves were obtained using a home-made testing device. External resistor (1–1000 Ω) was used for adjustment of the resistance. The corresponding current and voltage were recoded 5 s after the resistance was set. This allows for sufficient time for the voltage to reach stable status. The constant current test was acquired through an electrochemical workstation (eDAQ data acquisition systems) using galvanstatic testing mode. Impedance spectra were recorded in the frequency range of 0.1 Hz to 100 kHz using a sinusoidal amplitude modulation of ±5 mV about the open-circuit potential. Formic acid (88% Analytial grade, Enox®) was diluted with deionization water to give a suitable concentration ranging from 2 to 12 M.

4. Results and discussion

4.1. Effects of formic acid concentration on the cell performance

Fig. 4 shows the effects of formic acid concentration on the cell performance at different catalyst loadings. Changes of open-circuit voltage (OCV) with formic acid concentrations are plotted in Fig. 5. Generally, it can be seen that the cell OCV decreased with increased formic acid concentration. When the catalyst loading is 0.5 mg cm^{-2} for both the electrodes, the OCV decreased from 0.68 to 0.54 V. In comparison, the OCV dropped from 0.77 to 0.64 V when the loading increased to 1 mg cm^{-2}. This was due to the increased formic acid crossover rate from anode to cathode with increased concentration [7]. The formation of 'mixed potential', which was caused by the crossover of formic acid, lowered the cell OCV [24,34]. It can be observed from Fig. 6 that the maximum power density did not change linearly with the formic acid concentration increase: increased from 7.3 to 11.0 mW cm^{-2} when the formic acid concentration increased from 2 to 5 M for catalyst loading of 0.5 mg cm^{-2} for both the electrodes and increased from 15.2 to 19.6 mW cm^{-2} when the concentration changed from 2 to 8 M at a loading of 1 mg cm^{-2}. As the concentration further increased to 12 M, the maximum power density decreased obviously, at 2.5 and 12.2 mW cm^{-2} for a catalyst loading of 0.5 and 1 mg cm^{-2}, respectively. Similar results can be found by comparing the current densities at 0.5 V in Fig. 7. The current density increased from 9.7 to 10.8 mA cm^{-2} as the formic acid concentration increased from 2 to 5 M (at a catalyst loading of 0.5 mg cm^{-2}), and increased from 19.5 to 23.8 mA cm^{-2} when formic acid concentration changed from 2 to 8 M (at a catalyst loading of 1 mg cm^{-2}). When higher concentration (12 M formic acid) was fed into the cell, the current density dropped to only about 1.5 mA cm^{-2} and 11 mA cm^{-2} for a catalyst loading of 0.5 and 1 mg cm^{-2}, respectively. These observation differences are mainly attributed to the following three reasons:

(1) Fuel supply rate from the reservoir to catalyst is mainly dependant on the fuel concentration. In Fig. 4(a) and (b) when the fuel concentration is 2 M and 5 M, the cell performance is similar at low current densities (lower than 12 mA cm^{-2} in Fig. 4(a) and lower than 20 mA cm^{-2} in Fig. 4(b)). However, the feeding concentration affects the cell performance significantly at higher densities (higher than 12 mA cm^{-2} in Fig. 4(a) and higher than 20 mA cm^{-2} in Fig. 4(b)). The cell performance is better as the 5 M formic acid was fed. This is probably due to the fuel supply limitation at lower concentrations (2 M in this study). In order to overcome mass transfer resistances, higher concentrations are needed to reduce the diffusion force generated by the formic acid concentration gradients [35].

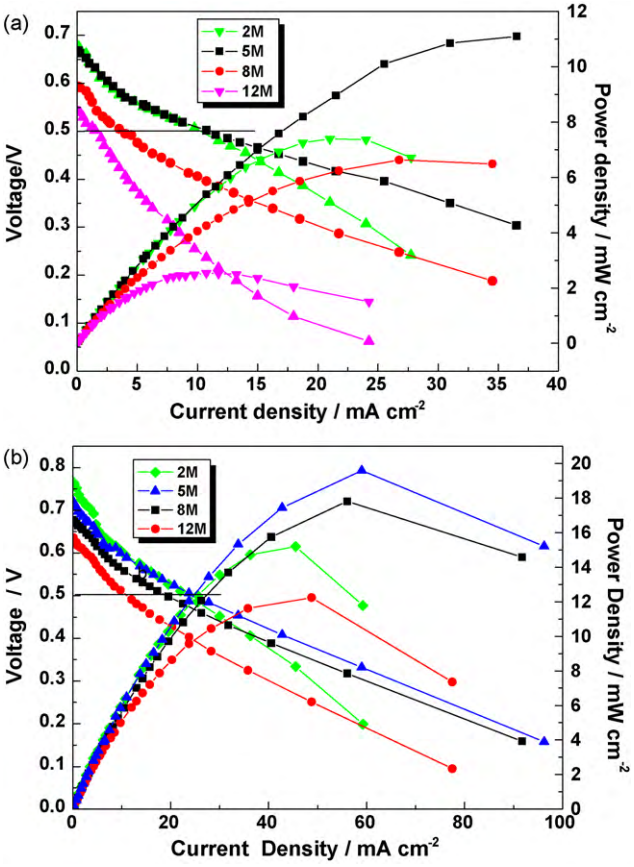

Fig. 4. Effects of formic acid concentration on the cell performance at different catalyst loadings: (a) 0.5 mg cm^{-2} Pd/C at the anode and 0.5 mg cm^{-2} Pt/C at the cathode and (b) 1 mg cm^{-2} Pd/C at the anode and 1 mg cm^{-2} Pt/C at the cathode.

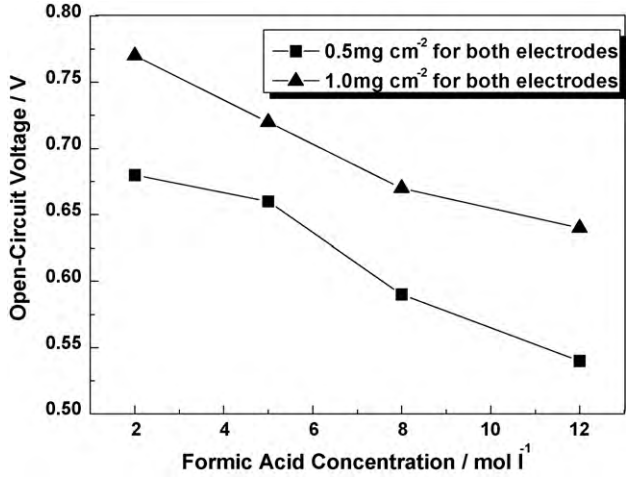

Fig. 5. Changes of the open-circuit voltage (OCV) with formic acid concentrations.

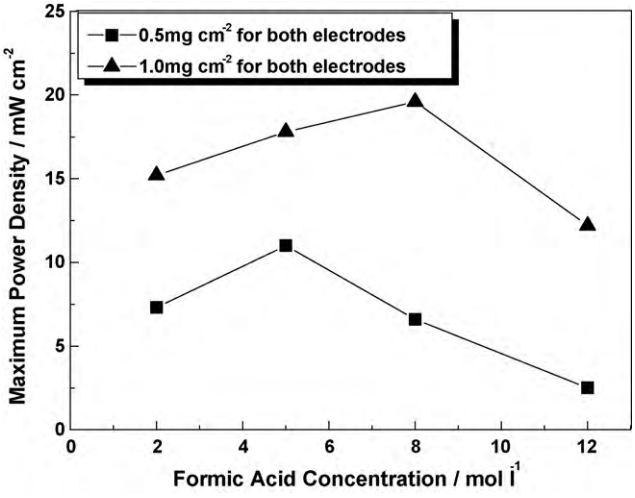

Fig. 6. Changes of the maximum power density with formic acid concentrations.

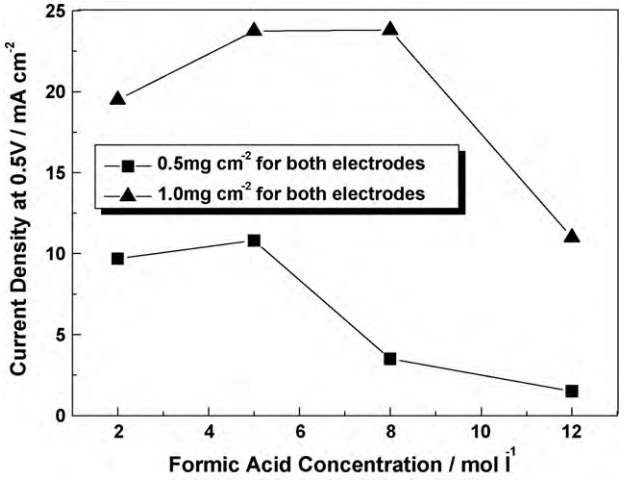

Fig. 7. Changes of current density at 0.5 V with formic acid concentrations.

(2) Fuel crossover rate, which is directly proportional to the fuel concentration. Generally higher concentration necessarily means higher fuel supply rate and higher fuel crossover as well [7,15]. It is understood that the reaction between the permeated formic acid and oxygen on the cathode is exothermic and heat generated by this reaction could result in an increase of cell operating temperature [34]. The increased temperature speeded up the reactions in both electrodes which is beneficent for the passive fuel cell. On the other hand, it should be noted that high fuel crossover could adversely poison the cathode Pt/C catalyst.

(3) Water content in the membrane, which affects the proton conductivity of the membrane. The largest contribution of internal resistance comes from the water content in the membrane [34]. Concentrated formic acid can induce membrane dehydration due to its hygroscopic nature, leading to deteriorated PEM performance. It can be observed that the cell performance was worst when 12 M formic acid was fed. The PEM had probably been deteriorated in such a highly concentrated fuel. It is very important for miniature fuel cells to operate in a dedicated balance between fuel supply, fuel crossover and water content in the membrane [36]. The experimental results in this study indicated that the optimized formic acid concentration is 5 M for the best passive DFAFC performance. A recent study also reported that the optimal concentration was *ca.* 6 M [37].

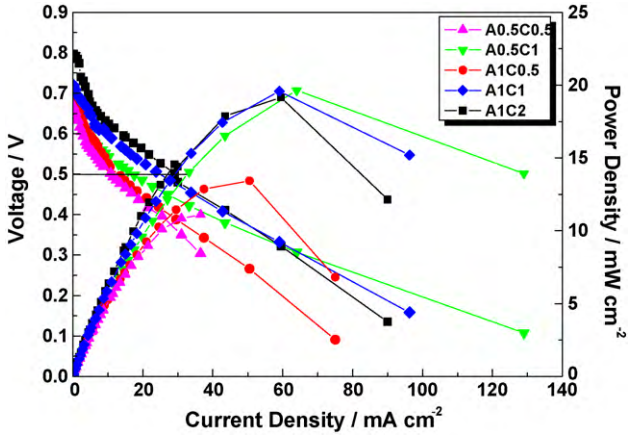

Fig. 8. Effects of catalyst loading on the cell performance (5 M HCOOH) (A*x*C*y* means: anode loading *x* mg cm^{-2} Pd/C and cathode loading *y* mg cm^{-2} Pt/C).

4.2. Effects of the catalyst loading on cell performance

Fig. 8 displays the effects of the catalyst loading on the performance of the cell. Pd/C loading at the anode and Pt/C loading at the cathode in the MEA varied from 0.5 to 2 mg cm^{-2}. The feeding fuel concentration was 5 M for this test. The cell performance was increased either by increasing the anode or cathode catalyst loadings. Comparing A1C1 with A1C0.5 and A0.5C1 with A0.5C0.5, the maximum power density and the current density at 0.5 V (Table 1) increased with increased catalyst loading in different degrees. When high catalyst loadings are used, more catalytic active sites are available for formic acid oxidation and oxygen reduction. Catalyst loading is also correlated with the connection between the catalyst layer and carbon paper: lower catalyst loading results in poor connection leading to larger connection resistance (Table 1). However, there is a ceiling limitation for loading increase. Too high loading would increase the mass transport resistance especially at high current density [14]. Comparing A1C2 with A1C1, the better performance of A1C2 relative to A1C1 at low current density (lower than 30 mA cm^{-2}) could be attributed to the more available catalytic active sites and suitable connection. Thick catalytic layer increased mass transport resistance at high current density (higher than 30 mA cm^{-2}), resulting in poor performance.

Fig. 9 presents the EIS of the cell with different catalyst loadings at the OCV after the *I–V* curves were obtained. Large resistances at the high frequency end were observable. The diameters of the capacitive circles were different with varying catalyst loadings. A large semicircular arc is indicative of large charge transfer resistance. It can be seen from Fig. 9 that A0.5C0.5 and A0.5C1 displayed

Table 1
Cell performance with varying catalyst loadings.

	A1C2	A1C1	A1C0.5	A0.5C1	A0.5C0.5
Maximum power density (mW cm^{-2})	19.1	19.6	13.4	19.6	10.8
Current density at 0.5 V (mA cm^{-2})	14.6	12.0	6.7	8.7	5.4
Internal resistance (Ω)	0.18	0.17	0.21	0.12	0.27

Table 2
Summary of the performance of some passive DFAFC in literatures under similar working conditions (JM: Johnson Matthey, OCP: open-circuit potential, MPD: maximum power density).

Ref.	Anode catalyst and loading	Cathode catalyst and loading	OCP (V)	MPD ($mW\,cm^{-2}$)	MPD normalized by anode catalyst ($mW\,cm^{-2}\,mg^{-1}$)
[23]	PtRu black (JM) 4 $mg\,cm^{-2}$	Pt black (JM) 12 $mg\,cm^{-2}$	0.80	33.0 at 0.17 V	8.3
[22]	Electrodeposited Pd 4 $mg\,cm^{-2}$	Electrodeposited Pt 2.5 $mg\,cm^{-2}$	0.60	12.3 at 0.24 V	3.1
[24]	Pd black (JM) 8 $mg\,cm^{-2}$	Pt black (JM) 8 $mg\,cm^{-2}$	0.85	178.0 at 0.53 V	22.2
[20]	Pd black (Sigma–Aldrich) 4 $mg\,cm^{-2}$	60 wt.% Pt/C (JM) 4 $mg\,cm^{-2}$	0.85	53.7 at 0.5 V	13.4
This work	Home-made Pd/C 1 $mg\,cm^{-2}$	40 wt.% Pt/C (JM) 1 $mg\,cm^{-2}$	0.72	19.6 at 0.35 V	19.6

large semicircular arc which may be correlated to their poor performance in Fig. 8.

4.3. The long-term performance test

Fig. 10 shows the long-term performance of the cell at constant current density. Experiment was conducted with 5 M formic acid as feeding and at a current density of 5 $mA\,cm^{-2}$. The catalyst loading is 1 $mg\,cm^{-2}$ at the anode and 2 $mg\,cm^{-2}$ at the cathode. It can be seen that the output voltage decreased quickly during the first few minutes, from 0.74 to 0.64 V. Thereafter, the degradation became very slow. During the whole recharging process, the voltage decreased from 0.64 to 0.51 V in 3 h. Possible reasons for cell performance degradation include the decrease of formic acid concentration, catalyst dissolution, fuel crossover and water accumulation at the cathode [8,20]. As is known, the passive DFAFCs are not equipped with fuel and oxygen feed pumps and fan that are used in a typical active fuel cells. Therefore it can be predicted that the fuel concentration decreases with fuel consumption leading to degraded performance. Secondly, with the long-term operation, water accumulation at the cathode, which was produced by oxygen reduction and the oxidation of crossed-over formic acid as well as water crossover from anode, caused an increase of oxygen transport constrain. Thirdly, the catalyst poisoning and Pd dissolution by formic acid were inevitable. Improvement on the long-term stability and reproducibility are the major goals in the future work.

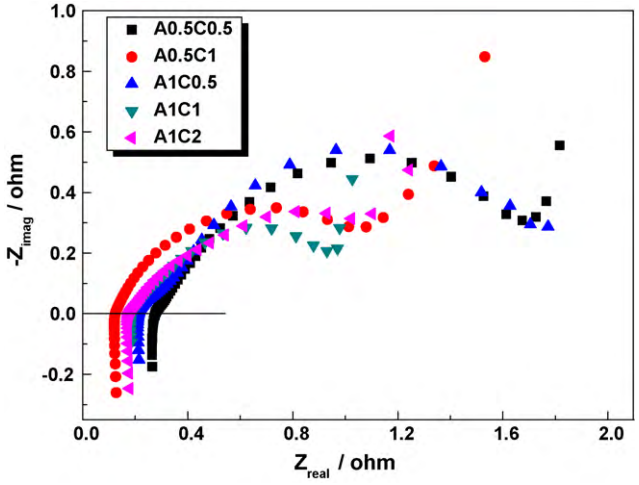

Fig. 9. Nyquist plots of the cell with varying catalyst loadings (5 M HCOOH).

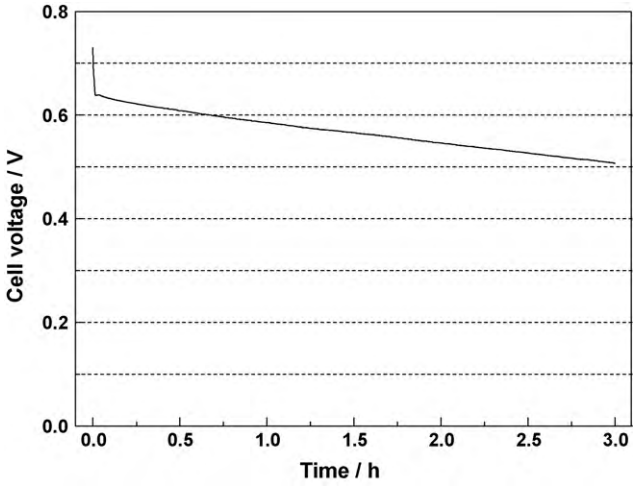

Fig. 10. Stability test of the cell at constant current density (5 $mA\,cm^{-2}$, 5 M HCOOH, 1 $mg\,cm^{-2}$ Pd/C at the anode and 2 $mg\,cm^{-2}$ Pt/C at the cathode).

It is perhaps noteworthy that the cell performance in terms of maximum power density in this work appears to be lower than those reported in literature. We figured out that the main reason is the low catalyst loading used in this work. Table 2 summarized the performance of some passive DFAFC in literatures under similar working conditions. It can be seen that the maximum power density normalized by anode catalyst loading in this work is not small at all.

5. Conclusions

A miniature air breathing DFAFC based on the PCB technology with an active area of 4 cm^2 was designed, fabricated and tested. The cell performance was evaluated with varying formic acid concentration and catalyst loading. It was found that the cell performance enhanced firstly with increased fuel concentration and then decreased. Similarly, catalyst loading increase led to enhanced power density at the beginning and then decreased with further increase of loading. A maximum power density of 19.6 $mW\,cm^{-2}$ was obtained with 5.0 M HCOOH and 1 $mg\,cm^{-2}$ catalyst loading at both the electrodes. The cell voltage decreased only about 20% (from 0.64 to 0.51 V) in 3 h at a constant discharging current density (5 $mA\,cm^{-2}$). It is therefore concluded that DFAFC based on PCB technology is viable for applications in portable market.

References

[1] J.-H. Kim, J.-Y. Lee, K.-H. Choi, H. Chang, J. Power Sources 185 (2008) 881–885.
[2] Y. Zhu, J. Liang, C. Liu, T. Ma, L. Wang, J. Power Sources 193 (2009) 649–655.
[3] S.H. Kim, H.Y. Cha, C.M. Miesse, J.H. Jang, Y.S. Oh, S.W. Cha, Int. J. Hydrogen Energy 34 (2009) 459–466.
[4] J.J. Martin, W. Qian, H. Wang, V. Neburchilov, J. Zhang, D.P. Wilkinson, Z. Chang, J. Power Sources 164 (2007) 287–292.
[5] D.J. Butler, Fuel cell today portable fuel cell survey, 2009.
[6] Q.Z. Lai, G.P. Yin, Z.B. Wang, C.Y. Du, P.J. Zuo, X.Q. Cheng, Fuel Cells 8 (2008) 399–403.
[7] K.-J. Jeong, C.M. Miesse, J.-H. Choi, J. Lee, J. Han, S.P. Yoon, S.W. Nam, T.-H. Lim, T.G. Lee, J. Power Sources 168 (2007) 119–125.
[8] X.W. Yu, P.G. Pickup, J. Power Sources 182 (2008) 124–132.
[9] Y. Zhu, S.Y. Ha, R.I. Masel, J. Power Sources 130 (2004) 8–14.
[10] U.B. Demirci, Environ. Int. 35 (2009) 626–631.
[11] S. Ha, R. Larsen, Y. Zhu, R.I. Masel, Fuel Cells 4 (2004) 337–343.
[12] S. Ha, C.A. Rice, R.I. Masel, A. Wieckowski, J. Power Sources 112 (2002) 655–659.

[13] C. Rice, S. Ha, R.I. Masel, P. Waszczuk, A. Wieckowski, T. Barnard, J. Power Sources 111 (2002) 83–89.
[14] J.S. Kim, J.K. Yu, H.S. Lee, J.Y. Kim, Y.C. Kim, J.H. Han, I.H. Oh, Y.-W. Rhee, Korean J. Chem. Eng. 22 (2005) 661–665.
[15] Y.-W. Rhee, S.Y. Ha, R.I. Masel, J. Power Sources 117 (2003) 35–38.
[16] S. Ha, R. Larsen, R.I. Masel, J. Power Sources 144 (2005) 28–34.
[17] R.F. Wang, S.J. Liao, S. Ji, J. Power Sources 180 (2008) 205–208.
[18] J.J. Wang, Y.G. Chen, H. Liu, R.Y. Li, X.L. Sun, Electrochem. Commun. 12 (2010) 219–222.
[19] C.M. Miesse, W.S. Jung, K.-J. Jeong, J.K. Lee, J. Lee, J. Han, S.P. Yoon, S.W. Nam, T.-H. Lim, S.-A. Hong, J. Power Sources 162 (2006) 532–540.
[20] Y.Y. Kang, M.J. Ren, T. Yuan, Y.J. Qiao, Z.Q. Zoa, H. Yang, J. Power Sources 195 (2010) 2649–2652.
[21] S. Uhm, Y. Kwon, S.T. Chung, J. Lee, Electrochim. Acta 53 (2008) 5162–5168.
[22] J. Yeom, R.S. Jayashree, C. Rastogi, M.A. Shannon, P.J.A. Kenis, J. Power Sources 160 (2006) 1058–1064.
[23] S. Ha, B. Adams, R.I. Masel, J. Power Sources 128 (2004) 119–124.
[24] S. Ha, Z. Dunbar, R.I. Masel, J. Power Sources 158 (2006) 129–136.
[25] Y.H. Chan, T.S. Zhao, R. Chen, C. Xu, J. Power Sources 178 (2008) 118–124.
[26] V. Baglio, A. Stassi, F.V. Matera, A. Di Blasi, V. Antonucci, A.S. Aricò, J. Power Sources 180 (2008) 797–802.
[27] N. Hashim, S.K. Kamarudin, W.R.W. Daud, Int. J. Hydrogen Energy 34 (2009) 8263–8269.
[28] Y.-D. Kuan, J.-Y. Chang, S.-M. Lee, S.-R. Lee, J. Power Sources 187 (2009) 112–122.
[29] Q.Z. Lai, G.P. Yin, Z.B. Wang, Int. J. Energy Res. 33 (2009) 719–727.
[30] H.S. Kim, R.D. Morgan, B. Gurau, R.I. Masel, J. Power Sources 188 (2009) 118–121.
[31] L. Jaeyoung, H. Jonghee, C.M. Miesse, J. Won Suk, J. Kyoung-Jin, L. Jae Kwang, Y. Sung Pil, N. Suk Woo, L. Tae-Hoon, H. Seong-Ahn, J. Power Sources 162 (2006) 532–540.
[32] L.M. Xu, S.J. Liao, L.J. Yang, Z.X. Liang, Fuel Cells 9 (2009) 101–105.
[33] Y.-N. Wu, S.-J. Liao, Z.-X. Liang, L.-J. Yang, R.-F. Wang, J. Power Sources 194 (2009) 805–810.
[34] S. Uhm, S.T. Chung, J. Lee, J. Power Sources 178 (2008) 34–43.
[35] D. Kim, E.A. Cho, S.-A. Hong, I.-H. Oh, H.Y. Ha, J. Power Sources 130 (2004) 172–177.
[36] S. Uhm, H.J. Lee, J. Lee, Phys. Chem. Chem. Phys. 11 (2009) 9326–9336.
[37] J.S.J. Ferrer, E. Couallier, M. Rakib, G. Durand, Electrochim. Acta 52 (2007) 5773–5780.